Research Article

Xiaochao Li, Handong Liu, Jishun Pan, Dongdong Li*, and Jin Wang

Rainfall thresholds of shallow landslides in Wuyuan County of Jiangxi Province, China

https://doi.org/10.1515/geo-2020-0120
received September 1, 2019; accepted April 11, 2020

Abstract: Rainfall is a critical factor inducing landslides, and thus the study of rainfall thresholds is of great significance for the prediction and prevention of landslides. In June 2017, infrastructures such as electric power pylons and roads were threatened by group-occurring landslides due to continuous heavy rainfall in Wuyuan County, Jiangxi Province of China. Based on the analysis of the rainfall data from March to September in this region, the lower (92.4 mm/d) and the upper (217.1 mm/d) empirical rainfall thresholds were determined. The soil water characteristic parameters of a typical landslide were determined by laboratory tests and back-analysis. Then, the factor of safety (FOS) versus time and the mechanical response of failure process with rainfall infiltration were examined. The results showed that during rainfall infiltration, the pore-water pressure increased, while the matrix suction and the stability decreased gradually. After the rain, the FOS increased slowly to a constant value, which was smaller than the initial. The physical rainfall threshold (200 mm/d), determined using 18 numerical simulation tests considering different rainfall intensities and amounts, was consistent with the empirical rainfall threshold. The methods developed in this work provide a useful tool for the prediction of landslides under extreme rainfall conditions.

Keywords: Wuyuan County, shallow landslides, rainfall thresholds, effective rainfall

*** Corresponding author: Dongdong Li,** School of Geosciences and Engineering, North China University of Water Resources and Electric Power; Henan Key Laboratory of Geotechnical and Structure Engineering, Zhengzhou 450045, China, e-mail: 741721553@qq.com, tel: +86-13938400450
Xiaochao Li: School of Geosciences and Engineering, North China University of Water Resources and Electric Power; Henan Key Laboratory of Geotechnical and Structure Engineering, Zhengzhou 450045, China; General Contracting Branch, Power Construction Corporation of China Jiangxi Electric Power Design Institute Co., Ltd, Nanchang 330096, China, e-mail: 347790530@qq.com
Handong Liu: School of Geosciences and Engineering, North China University of Water Resources and Electric Power; Henan Key Laboratory of Geotechnical and Structure Engineering, Zhengzhou 450045, China, e-mail: Liuhandong@ncwu.edu.cn
Jishun Pan: School of Geosciences and Engineering, North China University of Water Resources and Electric Power; Henan Key Laboratory of Geotechnical and Structure Engineering, Zhengzhou 450045, China, e-mail: Panjishun@ncwu.edu.cn
Jin Wang: Chengdu Xingcheng Construction Management Co., Ltd., Chengdu Xingcheng Investment Group Limited, Chengdu 610031, China, e-mail: 251399112@qq.com

1 Introduction

Landslides induced by rainfall, posing a great threat to lives and infrastructures in mountain areas, have received increased attention in recent decades [1–8]. Thus, quantifying the triggering rainfall thresholds in a region will be of great importance in risk assessments and early warning of landslide hazards.

The relationship between rainfall and landslides is affected by several factors, such as rainfall intensity, rainfall duration, accumulated rainfall, antecedent accumulated rainfall, and geomorphologic and geological characteristics of a slope [9–15]. Thus, an effective method to study this dependence is essential. The widely used methods of threshold definition are the basic concept method [13,16,17] and the statistical method [17–22]. For the basic concept method, the thresholds were drawn manually by delimiting the lower bound of the point cloud representing the triggering rainfall conditions or by searching the best fit of the lower part of the cloud [13]. While the statistical method was conducted by establishing the relationship between rainfall conditions and rainfall thresholds based on the principles of statistics. Many triggering rainfall thresholds have been established for early warning of rainfall-induced landslides in different regions, depending on the statistical analysis of historical landslide records and the corresponding rainfall conditions [18,23–35]. The previous studies on triggering rainfall thresholds focused on the statistical analysis of rainfall events and landslides, and little attention was paid to the failure mechanism of rainfall-induced landslides [36–38]. In

recent years, a synthetic approach has been adopted in many studies, combining the physical failure mechanism with empirical approaches [26,37,39,40].

Jiangxi Province is a region with high susceptibility to landslides in Southeast China. The number of landslides has reached 6,634 according to the Geological Hazard Survey of 35 counties in Jiangxi, among which the rainfall-induced landslides account for 79.7% [41]. However, few studies on triggering rainfall thresholds of shallow landslides are found for this region. Due to the lack of early warning, many infrastructures were threatened by rainfall-induced landslides, as shown in Figure 1, when a heavy rainfall storm hit Wuyuan on June 23–24, 2017, a county town in northeast Jiangxi. The aim of this study is to determine a regional rainfall threshold for Wuyuan County, Jiangxi Province, China, to enhance the capacity for early warning of landslide hazards. First, the empirical rainfall thresholds were determined by statistical analysis of rainfall data from March to September, 2017, in this area. After that, characteristics of rainfall infiltration and variation of unsaturated soil shear strength under rainfall were analyzed. Finally, the physical rainfall threshold was determined by analyzing the mechanisms of rainfall infiltration and slope failure processes, considering the regional geotechnical and hydrological conditions. The lower and upper empirical rainfall thresholds were proposed for the first time in Wuyuan County using synthetic methods.

2 Materials and methods

2.1 Study area

Wuyuan County is located in the southeast of Jiangxi Province, China, with a total land area of about 2,950 km^2 (Figure 2). The topography of Wuyuan comprises steep mountainous areas and dissected valleys. The highest point is Leigujian Shan (1629.8 m) in the northeast. Other prominent topographic features include Huangjing Peak (507 m) in the middle and Miaobaowu Peak (233 m) in the southwest (Figure 2).

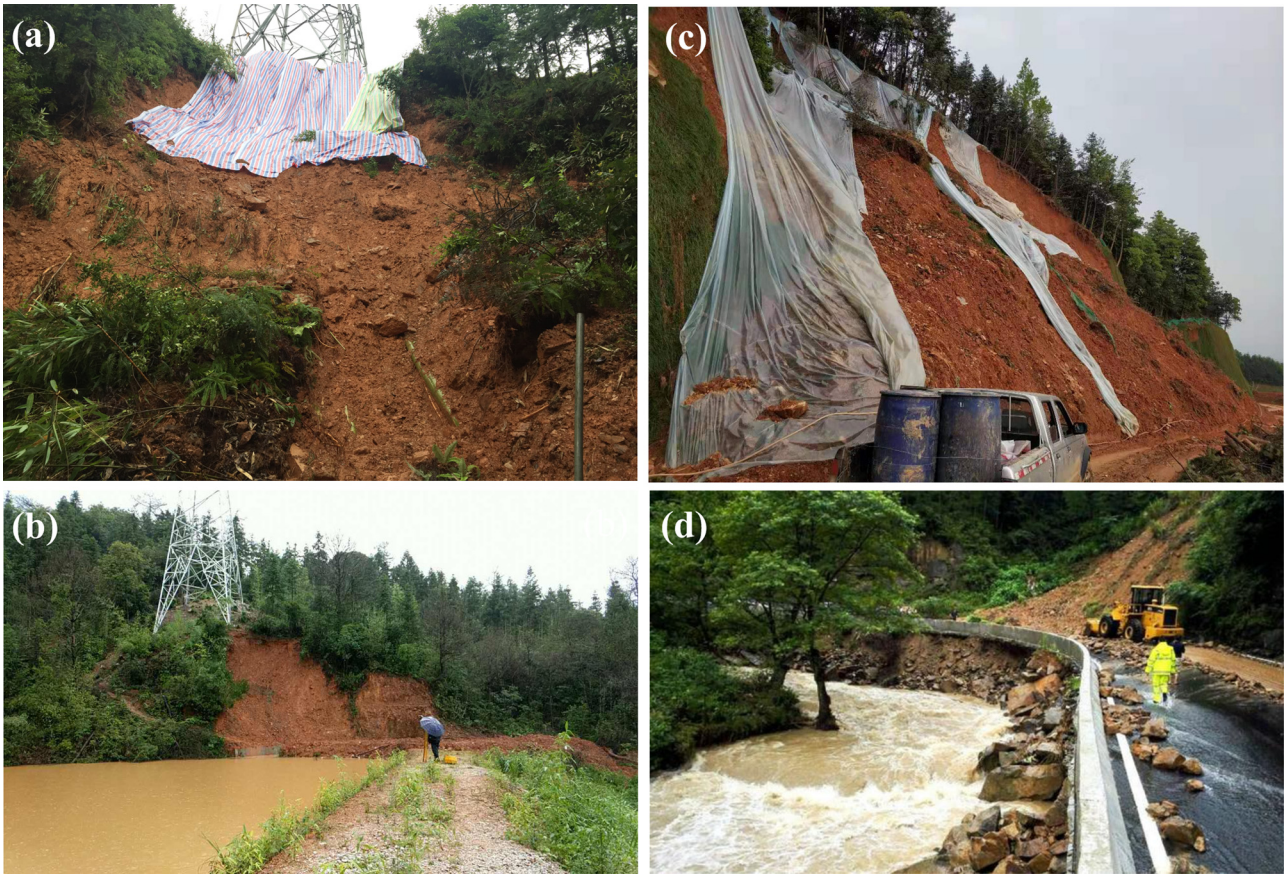

Figure 1: Infrastructures threatened by rainfall-induced landslides in Wuyuan County on June 23–24, 2017 ((a and b) landslides nearby electric power pylons; (c and d) landslides along roads, photos were taken by Xiaochao Li).

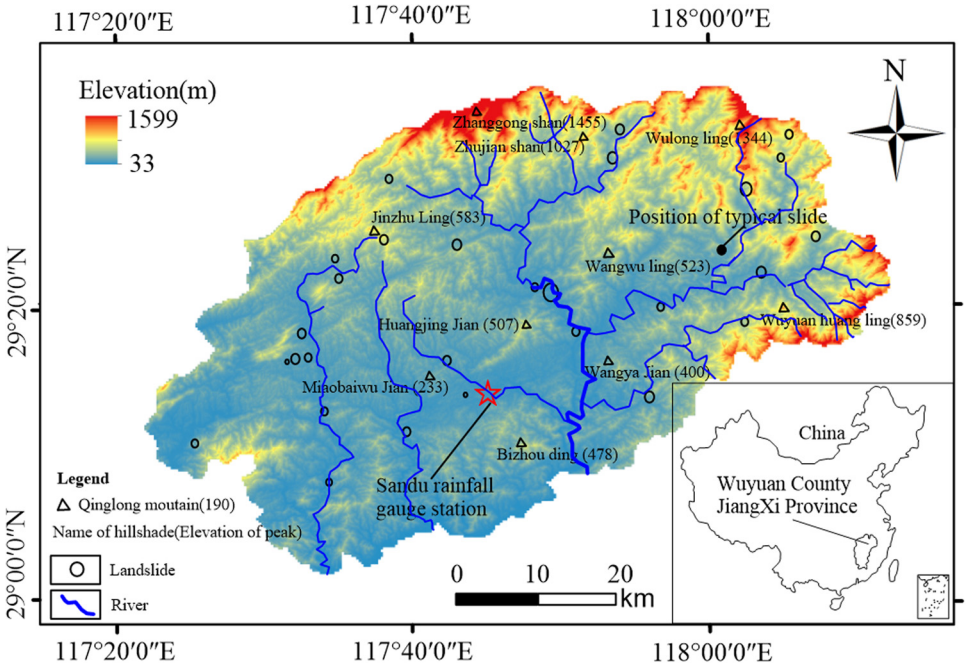

Figure 2: Topography of Wuyuan County (position of landslides from Dr. Xiaochao Li's emergency response).

A mountainous terrain with steep slopes occupies about 83% of the land. The rivers in the study area are densely distributed, and the main flow direction is from the northwest to the southeast. The main strata in the study area can be grouped into two categories [42]. One is the pre-Sinian System Shuangqiaoshan Group AnZzsh^2, which mainly contains phyllitic slate and phyllitic sediment-tuff. The other is the Cretaceous System Shixi Group $K_{1\text{-}s}$, including mudstone, shale, and sandstone. An overview of the two strata units is presented in Figure 3. The older category covers most of the regions with a phyllitic structure or a stratified primary structural plane, which leads to the poor weathering ability of the bedrock and forms a weak structural surface. Simultaneously, shallow residual soil has a goodwater retention capability.

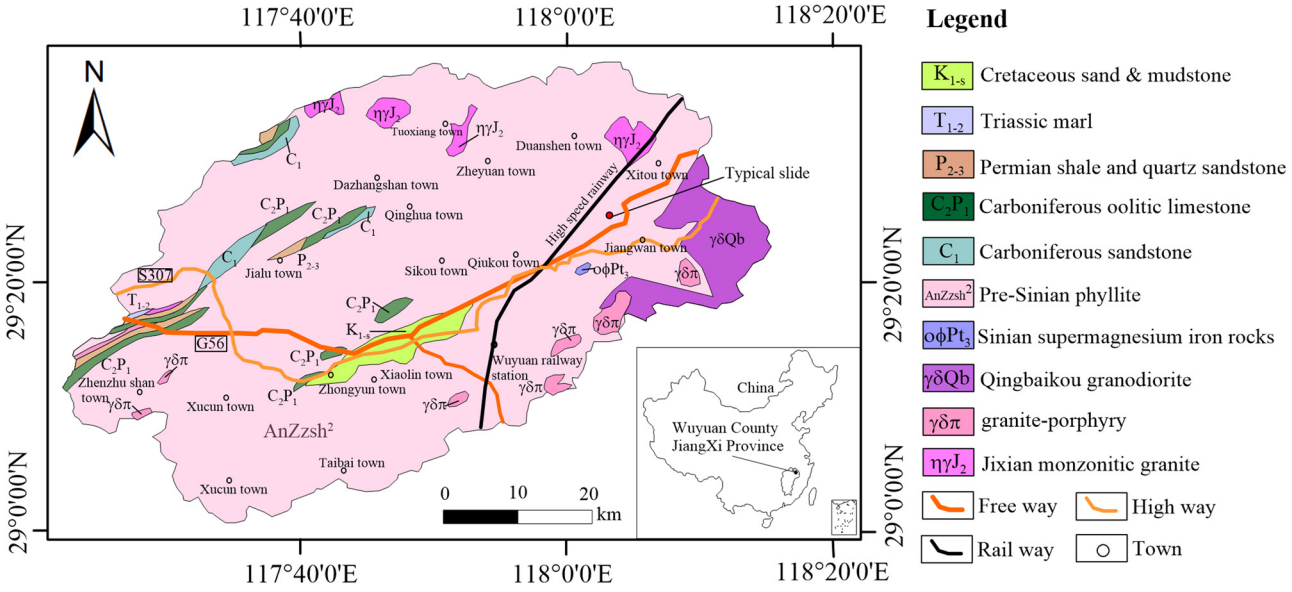

Figure 3: Regional geology map of the study area.

Wuyuan County has the humid monsoon climate of central Asia with the characteristics of the East Asian monsoon region. There are abundant rainfall and short frost periods in this region. The monthly rainfall increases from January to June and decreases from July to December every year. The average annual rainfall equals 1962.3 mm, 69% of which takes place in the first half-year. During the rainy season (from April to June), the average monthly rainfall reaches >300 mm. The cumulative rainfall in the rainy season accounts for 47.9% of the annual precipitation. The maximum monthly and daily precipitations occurred in July 1998 and reached 970.4 and 269.8 mm, respectively.

Large areas of Wuyuan County are prone to landslide processes, due to the geological setting and seasonal rainfall. In general, these rainfall-induced shallow landslides with a depth of 1–5 m, a length of 5–20 m and a material volume of 10–300 m^3 were produced on steeply dipping slopes (30–50°). The material involved in mass movement processes consists of saprolite and colluvium.

2.2 Rainfall data and effective rainfall model

The daily precipitation from March to September in 2017 was measured from the Sandu hydrological station and meteorological bureau (Figure 4). Evidently, the maximum daily rainfall (115.2 mm/d) and landslide occurred on the same day (June 24).

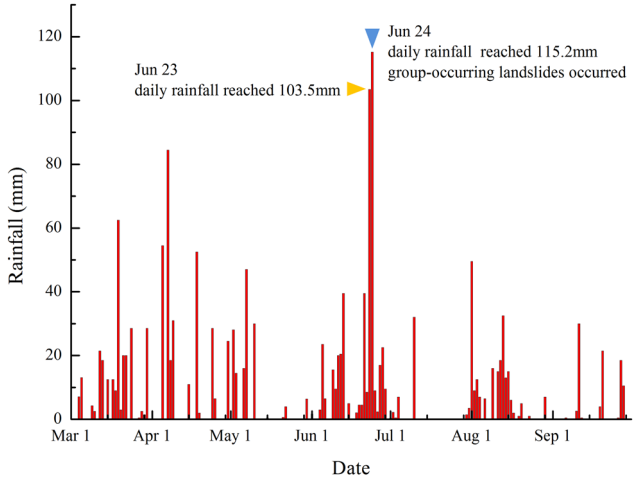

Figure 4: Variation of daily precipitation from March to September in 2017 in Wuyuan County.

As an extremely important parameter to determine rainfall threshold, the cumulative rainfall of each rainfall event was calculated (Table 1). One rainfall event began when the rainfall lasted for more than 1 day. However, the accumulated rainfall has a variable duration, so there is no uniform standard and the metric is not very convenient in practice. Converting the accumulated rainfall into effective daily rainfall is a recommended method to normalize the time factor of cumulative rainfall. Yin et al. proposed a model to calculate the effective rainfall, in which the rainfall coefficient (attenuation coefficient) played a key role [43]. The effective rainfall (R_e) is calculated as follows:

$$R_e = R_0 + \sum_{i=1}^{n} \lambda^i R_i \quad (1)$$

where R_0 is the rainfall on the day of landslides, n is the number of days of rainfall events, R_i is the daily rainfall before landslides, and λ is the rainfall coefficient.

The physical significance of λ is clear. It indicates that the effect of rainfall on the disaster gradually diminishes with time and eventually disappears. Shan [44] studied 115 rainfall-induced landslides from 1970 to 1999 in Jiangxi Province and determined the rainfall coefficient (λ) to be 0.75. Chen et al. [41] took λ to be 0.82 by studying 1,158 rainfall-induced landslides from 1973 to 2002 in Jiangxi Province. The smaller λ of 0.75 was chosen in this study.

2.3 Numerical equations of unsaturated soil

For the shallow landslides caused by rainfall, the sliding surface is mostly along the bedrock surface. Studies on the failure mechanism of rainfall-induced landslides mainly target the process of rainfall infiltration and the strength of unsaturated soil. In general, rainfall infiltration leads to an increase of pore-water pressure and a decrease of matrix suction in an unsaturated slope, which further results in a reduction in the shear strength of the soil [11,38,45,46]. The following shows the equations of rainfall infiltration in unsaturated soil and the corresponding constitutive model.

2.3.1 Partial differential equation of seepage in unsaturated soil

For unsaturated soil, the coefficient of permeability is not always a constant. The permeability coefficient

Table 1: Rainfall values exceeding 10 mm recorded from March to September in 2017 in Wuyuan County

Event no.	Start	End	Duration (d)	Cumulative (mm)	Event no.	Start	End	Duration (d)	Cumulative (mm)
1	Mar. 12th	Mar. 13th	2	40.0	11	May 10th	May 10th	1	30.0
2	Mar. 17th	Mar. 22nd	6	127.0	12	Jun. 4th	Jun. 6th	3	33.0
3	Mar. 24th	Mar. 24th	1	28.5	13	Jun. 9th	Jun. 15th	7	110.2
4	Mar. 27th	Mar. 30th	4	33.0	14	Jun. 18th	Jun. 29th	12	338.2
5	Apr. 5th	Apr. 5th	1	54.5	15	Jul. 10th	Jul. 10th	1	32.0
6	Apr. 7th	Apr. 9th	3	134.0	16	Jul. 30th	Aug. 4th	6	83.0
7	Apr. 18th	Apr. 18th	1	52.5	17	Aug. 11th	Aug. 17th	7	102.0
8	Apr. 24th	Apr. 25th	2	35.0	18	Sep. 10th	Sep. 11th	2	32.6
9	May 2nd	May 3rd	2	42.6	19	Sep. 19th	Sep. 20th	2	25.5
10	May 6th	May 7th	2	63.0	20	Sep. 27th	Sep. 28th	2	29.0

Note: The daily rainfall of Apr. 7th is 84.5 mm.

decreases with the decrease of water content in unsaturated soil. When water flows through two-dimensional unsaturated soil, the governing equation is adopted as follows [47,53]:

$$\frac{\partial}{\partial x}\left(-k_x\frac{\partial h_w}{\partial x}\right)+\frac{\partial}{\partial y}\left(-k_y\frac{\partial h_w}{\partial y}\right)+q=m_w^2\gamma_w\frac{\partial h_w}{\partial t} \quad (2)$$

where m_w^2 is the slope of the soil water characteristic curve (SWCC), h_w is the total hydraulic head, k_x is the water permeability relevant to matrix suction in the x-direction, k_y is the water permeability relevant to matrix suction in the y-direction, γ_w is the unit weight of water, q is the applied flux at the boundary, and t is the flow time.

2.3.2 Stress–strain relationship of unsaturated soil

Fredlund and Rahardjo [47] studied the stress–strain relation of unsaturated soil and proposed its incremental form as:

$$\{\Delta\sigma\}=[D]\{\Delta\varepsilon\}-[D]\{m_H\}(\sigma_a-u_w)+\{\Delta u_a\}. \quad (3)$$

Suppose that the atmosphere is a constant, equation (3) can be simplified as:

$$\{\Delta\sigma\}=[D]\{\Delta\varepsilon\}+[D]\{m_H\}u_w. \quad (4)$$

The stress–strain finite element equation can be obtained based on the virtual work principle,

$$\sum[B]^T[D][B]\{\Delta\delta\}+\sum[B]^T[D][B]\{m_H\}N\{u_w\}=\sum F. \quad (5)$$

Equation (5) can be written in another form:

$$[K]\{\Delta\delta\}+[L_d]\{\Delta u_w\}=\Delta F \quad (6\text{-}1)$$

$$\{m_H\}^T=\left(\frac{1}{H}\frac{1}{H}\frac{1}{H}0\right), \quad (6\text{-}2)$$

where $[K]=\sum[B]^T[D][B]$ is the stiffness matrix, $[B]$ is the strain matrix, $[D]$ is the drainage constitutive matrix, $[L_d]=\sum[B]^T[D][B]\{m_H\}N$ is the coupled matrix, $\{\Delta\delta\}$ is the incremental displacement vector, and $\{\Delta u_w\}$ is the incremental pore-water pressure vector.

2.3.3 Failure criteria of unsaturated soil

Fredlund and Rahardjo [47] proposed an extended Mohr–Coulomb failure criterion, in which the matrix suction of unsaturated soil was considered. Slope stability analysis was carried out using this equation after solving transient seepage. The equation is as follows:

$$\tau=c'+(\sigma_n-u_a)\tan\varphi'+(\sigma_a-u_w)\tan\varphi^b, \quad (7)$$

where τ is the shear strength of unsaturated soil, c' is the effective cohesion, (σ_n-u_a) is the net normal stress, σ_n is the total normal stress, u_a is the pore-air pressure, φ' is the effective angle of internal friction, (σ_a-u_w) is the matrix suction, u_w is the pore-water pressure, and φ^b is the angle indicating the rate of change in shear strength associated with matrix suction.

2.4 Numerical model and soil properties

Numerical simulation is an effective tool to reveal the mechanical response of slope under rainfall infiltration [48–52]. The landslide near the 83# iron tower of the Ziyang II 220 kV overhead transmission line is a typical case in Wuyuan County. Based on the geotechnical investigation report and reinforcement scheme, a numerical model and boundary conditions were built in SEEP/W, SIGMA/W, and SLOPE/W to simulate the mechanism of

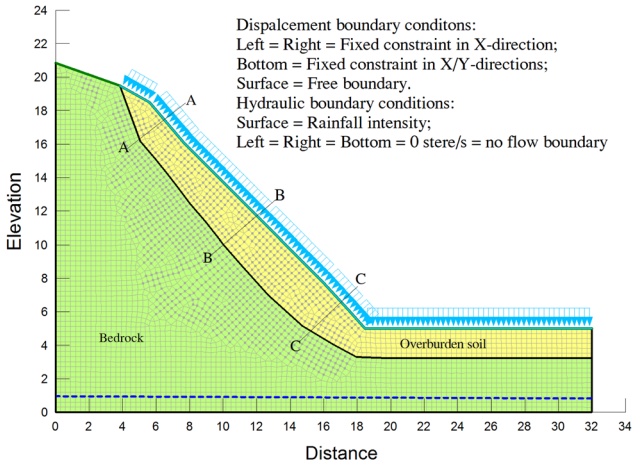

Figure 5: Slope geometry and boundary conditions; units: m (A–A, B–B, and C–C represent different sections along the slope).

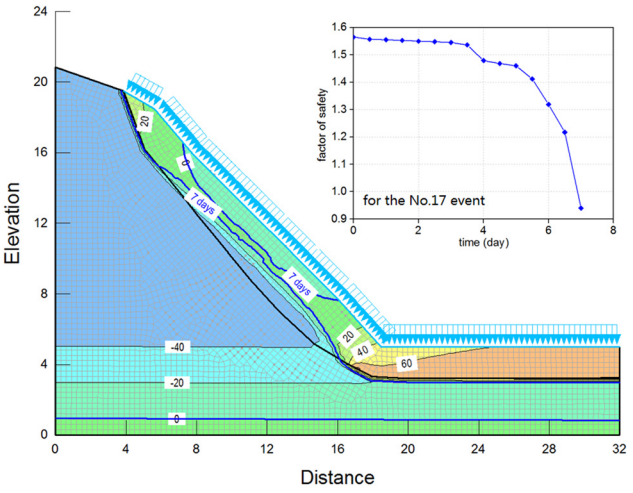

Figure 6: The seepage field at the moment of failure and the FOS versus time.

deformation and failure process under rainfall. The slope model is shown in Figure 5, which consisted of two types of materials. The upper one was overburden soil of about 2.5 m thickness and the lower one was bedrock (intensely weathered phyllitic slate). The model had a length of 32 m and an altitude of 20.85 m. The maximum elevation difference of the slope was 15.85 m and the angle of the slope was about 46°.

These simulations were conducted as follows. (1) The transient seepage analysis was performed by applying rainfall boundary on the slope surface in the SEEP/W program. (2) The time-dependent pore-water pressure determined from SEEP/W was coupled with SIGMA/W to obtain the stress–strain field. (3) The transient seepage and stress–strain analysis were used in SLOPE/W as a parent analysis to study the variation of the factor of safety (FOS) and slope deformation with time. In this process, the slip surface was fully specified according to the field survey, and the general limit equilibrium was used for slope stability analysis based on the finite element method.

The SWCC is an essential element in the transient seepage and stability analysis of unsaturated soil. In order to obtain the SWCC of the overburden soil, the technique of back-analysis was used on the basis of rainfall Event 14. Fredlund and Xing [53] proposed a general equation for the SWCC, which provided a good fit for sand, silt, and clay soils over the entire suction range from 0 to 10^6 kPa. A series of initial values were applied to the numerical model in terms of the general equation of the SWCC, and the numerical failure moment was compared with the real one. Then the unsaturated soil parameters were adjusted until the failure moments became consistent. The simulation started from the beginning of Event 14. The back-analysis results are presented in Figure 6. The FOS decreased with the daily rainfall intensity. On the seventh day, the slope was almost saturated and its FOS was below 1.0. The properties and the physical–mechanical indexes of soil or rock are listed in Table 2.

3 Results and discussion

3.1 Empirical rainfall thresholds

Many field inspections are performed each year by the State Grid of Jiangxi and other infrastructure departments (i.e., highway related and hydraulic related) in Wuyuan County. The inspection results show that there have not been group-occurring landslides in recent years except for the disaster on June 24, 2017. As shown in Table 1, a rainfall intensity of 84.5 mm/d and an accumulated rainfall of 134.0 mm cannot trigger group-occurring landslides, but a rainfall intensity of 115.2 mm/d and a total rainfall of 277.8 mm (June 18–24) could undoubtedly trigger group-occurring landslides. According to Chen et al. [41], when the accumulated rainfall is <63 mm, landslides rarely occur in the Jiangxi Province. Therefore, 7 of the 24 events with rainfall exceeding 63 mm were selected for further analysis. For Event No. 14, the time of failure was June 24, R_0 was 115.2 mm/d, n was 6, and R_i was daily rainfall from 18 to 23 June. Therefore, the result of effective rainfall was 217.1 mm/d. Similarly, the effective rainfall was calculated for Event No. 2, 6, 10, 13, 16, and 17, as shown in Table 3. Although the accumulated rainfall of these events was

Table 2: Parameters of soil and rock

Layer	Parameters					
	γ (kN/m^3)	c (kPa)	φ (degrees)	φ^b (degrees)	k_{sat} (cm/s)	μ
Overburden soil	19.5	10	20	Vol. WC fn.	8.68×10^{-5}	0.3
Intensely weathered phyllitic slate	20.2	35	30	—	1.16×10^{-7}	0.25
Soil water characteristic values	Overburden soil: a= 40 kPa, n = 1, m = 0.8, Sat. WC = 0.4; bedrock: a = 4.5 kPa, n = 1, m = 0.9, Sat. WC = 0.25					

large, the effective rainfall was not large enough to trigger landslides.

According to the above analysis, a lower effective rainfall threshold of 92.4 mm/d was determined, below which group-occurring landslides would not occur. Meanwhile, an upper effective rainfall threshold of 217.1 mm/d was determined, above which landslides always occurred. If the effective rainfall was in the range of 92.4 to 217.1 mm/d, the change of matrix suction and geological conditions should be considered to decide whether a landslide would occur or not.

3.2 Mechanical response of failure process with rainfall infiltration

Eighteen tests in three groups were designed to study the effects of total rainfall and intensity on slope stability, as shown in Table 4. According to the analyses above, the upper and lower empirical rainfall thresholds were 217.1 and 92.4 mm/d, respectively. Therefore, the total rainfall range from 140 to 240 mm with an interval of 20 mm was considered in this study. Furthermore, to assess the impact of rainfall intensity, the total rainfall was assumed to end within 24, 16, and 8 h of one day. In order to fully consider the influence of rainfall infiltration on slope stability, the calculation time was set to 10 days in the analysis process. The variations of pore-water pressure over time at different depths of Section-A, B, and C (Figure 5) are shown in Figure 7.

For Section-A, located at the upper part of the landslide, the pore-water pressure increased rapidly from an initial value of −50 kPa to nearly −5 kPa in 30 h. On the tenth day, the pore-water pressure gradually recovered to the initial value within 1.2 m depth, while it was slightly larger than the initial value under 1.2 m depth. For Section-B, the pore-water

Table 3: The effective rainfall of some important events from March to September in 2017 in Wuyuan County

Event no.	Cumulative rainfall (mm)	Effective rainfall (mm/d)	Event no.	Cumulative rainfall (mm)	Effective rainfall (mm/d)
2	127.0	68.9	6	134.0	92.4
10	63.0	59.0	13	110.2	47.3
14	277.8	217.1	16	83	43.8
17	102.0	37.7	Apr. 7th	84.5	84.5

Table 4: The minimum FOS of different numerical tests

Group	Duration (h)	Total rainfall (mm)					
		I	II	III	IV	V	VI
		140	160	180	200	220	240
A	24	1.107	1.068	1.054	1.035	1.012	0.935
B	16	1.059	1.063	1.026	0.989	0.980	0.929
C	8	1.065	1.056	1.051	0.967	0.938	0.914

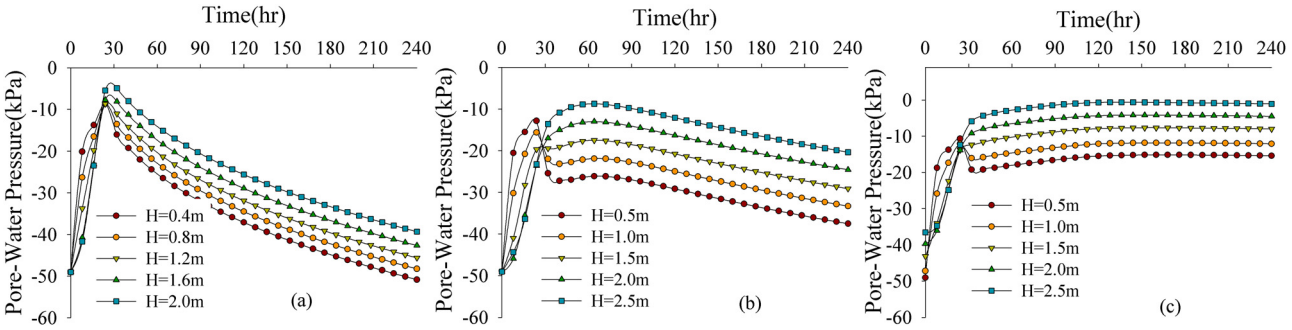

Figure 7: The variation of pore-water pressure over time: (a) Section-A, (b) Section-B, and (c) Section-C (Figure 5). Test A-IV is taken for example.

pressure increased rapidly from −50 kPa to nearly −10 kPa in 30 h within 1.0 m depth, and then decreased quickly to a relatively stable value in a short time. However, the bottom part of Section-B reached a maximum value of −10 kPa in 60 h, and then declined slowly to −15 kPa. For Section C, the pore-water pressure increased to a maximum value at different depths in 30 h and then stayed at this level. The pore-water pressure

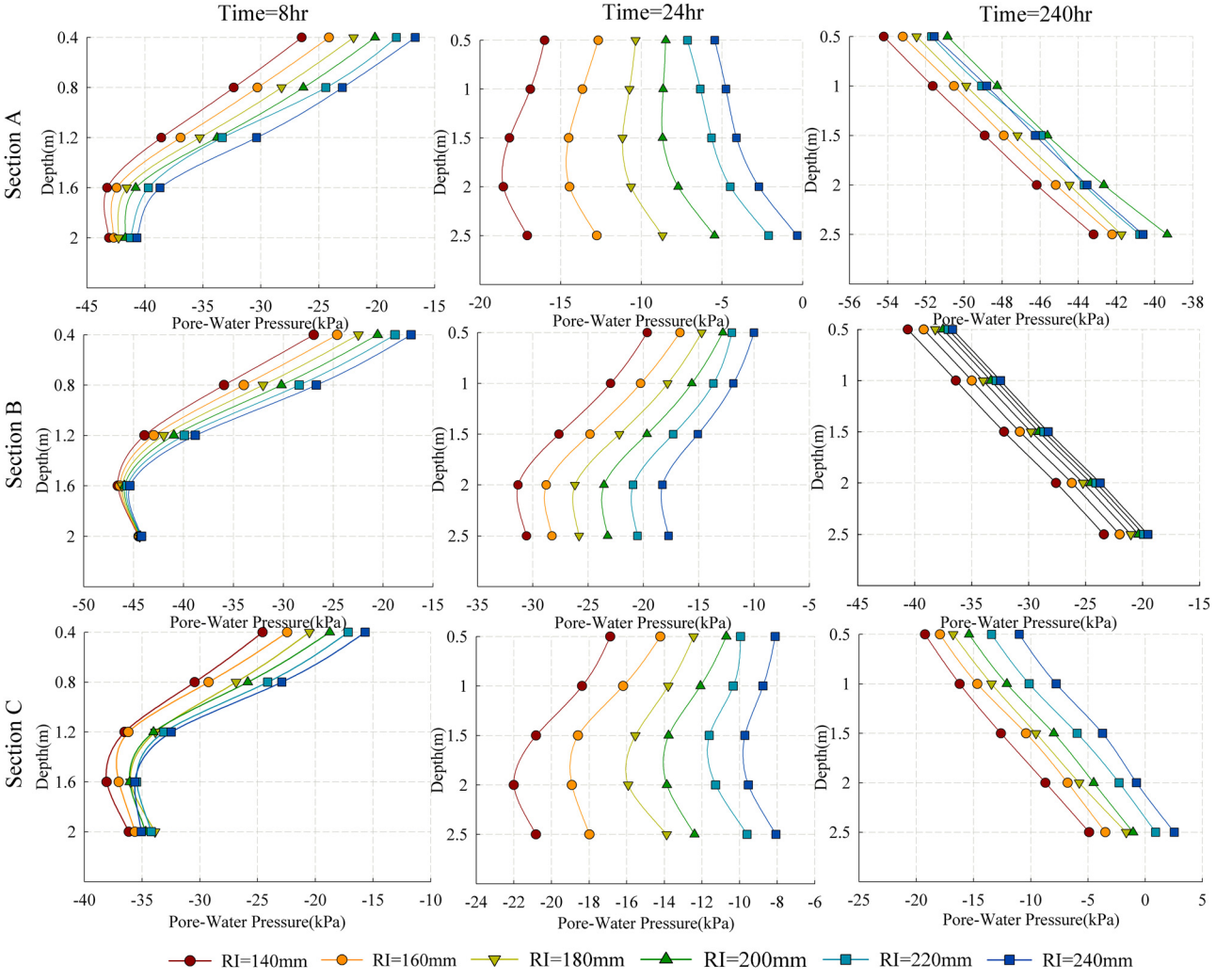

Figure 8: Pore-water pressure at different depths in the test of group-A (RI means the rainfall amount within 24 h).

increased continuously during the rainfall, which was consistent with the law of rainfall infiltration. The variation of pore-water pressure indicated that water permeated from the surface to the deep part, and from the top to the bottom of the slope.

The variation of pore-water pressure at different depths with different rainfall intensities is shown in Figure 8. The variation trend of pore-water pressure is similar for different rainfall intensities. With the increase of rainfall intensity, the pore-water pressure at the same depth also increased. At the beginning of the rainfall (T = 8 h), the pore-water pressure of shallow soil changed more significantly than the deep part with the increasing rainfall intensity. When the rain stopped (T = 24 h), the pore-water pressure of the whole slope increased, while the change at the bottom was more remarkable. Nine days later (T = 240 h), the pore-water pressure of Section-A nearly recovered to the initial value, and Section-C still maintained at a high level. The process of rainfall infiltration was well revealed by the variation of pore-water pressure. When the rainfall intensity increased to a critical value, the shear strength became smaller than the shear stress on the slide surface and landslides would occur.

3.3 FOS and physical rainfall threshold

The FOS versus time for three groups of tests is shown in Figure 9 and the minimum FOS of each test is listed in Table 4. The slope stability decreased continuously with the increase of rainfall and reached the minimum within 8 h after the rain. After that, the pore-water pressure decreased as the water drained and the FOS increased slowly to a new constant, which was smaller than the initial one. When the total rainfall was smaller than 200 mm, the FOS values of each test of the three groups were all greater than 1.0. But, when the total rainfall reached 200 mm, the FOS of test B-IV was 0.989.

In this article, the slope was considered failed when the FOS was below 1.0, and the corresponding rainfall was determined as the physical rainfall threshold. Therefore, the physical rainfall threshold is proposed to be 200 mm/day in Wuyuan County.

4 Conclusions

In this study, the rainfall thresholds were analyzed based on empirical and physical methods in Wuyuan County, considering the group-occurring landslides induced by rainfall. The results showed that the lower and upper empirical rainfall thresholds were 92.4 and 217.1 mm/d, respectively. When the rainfall was less than 92.4 mm/d, group-occurring landslides were not observed. When the rainfall was greater than 217.1 mm/d, landslides always occurred. If the rainfall was in the window interval (92.4–217.1 mm/d), the change of matrix suction and geological conditions should be considered. Eighteen numerical simulation tests considering different rainfall intensities and rainfall amounts were conducted. The process of rainfall infiltration was well revealed by the variation of pore-water pressure. The FOS decreased rapidly with the rain. After the rain, the soil matrix suction and the FOS gradually recovered because the water discharged out of the slope. The numerical results also showed that the physical rainfall threshold of Wuyuan was 200 mm/d, similar to the empirical rainfall threshold (217.1 mm/d) determined by the empirical method. Therefore, an effective rainfall of 200 mm/d could be regarded as the threshold that would trigger group-occurring shallow landslides in this area. The results of this study can provide useful information in the framework of landslide risk management. However, parameters of the SWCC used to determine the physical rainfall threshold, which were obtained by back-analysis, need to be supplemented by more *in situ* and laboratory tests.

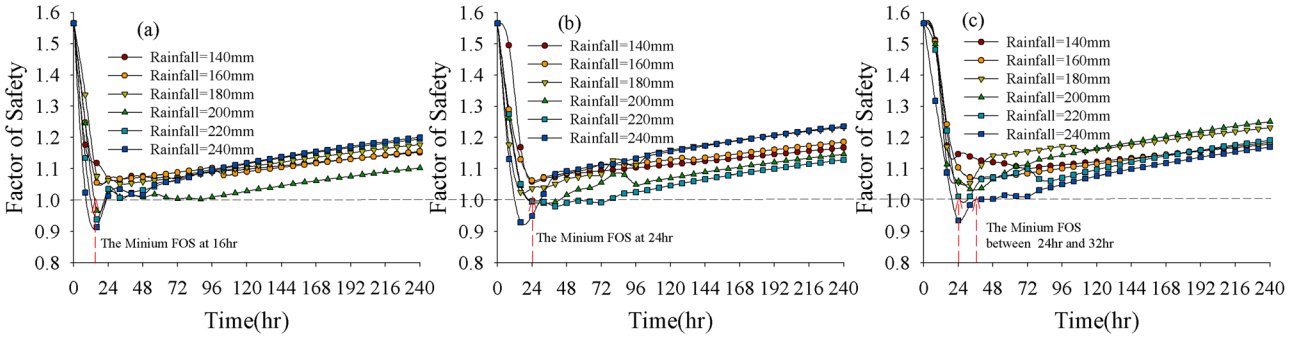

Figure 9: FOS versus time. (a) Rainfall duration = 8 h, (b) rainfall duration = 16 h, (c) rainfall duration = 24 h.

Acknowledgments: This work was supported by the National Natural Science Foundation of China (Grant No. U1704243).

Reference

[1] Sabatakakis N, Koukis G, Mourtas D. Composite landslides induced by heavy rainfalls in suburban areas: City of Patras and surrounding area, western Greece. Landslides. 2005;2:202–11.
[2] Yamagishi H, Iwahashi J. Comparison between the two triggered landslides in Mid-Niigata, Japan by July 13 heavy rainfall and October 23 intensive earthquakes in 2004. Landslides. 2007;4:389–97.
[3] Pánek T, Brázdil R, Klimeš J, Smolková V, Hradecký J, Zahradníček P. Rainfall-induced landslide event of May 2010 in the eastern part of the Czech Republic. Landslides. 2011;8:507–16.
[4] Chung MC, Tan CH, Chen CH. Local rainfall thresholds for forecasting landslide occurrence: Taipingshan landslide triggered by Typhoon Saola. Landslides. 2017;14:19–33.
[5] Senthilkumar V, Chandrasekaran SS, Maji VB. Geotechnical characterization and analysis of rainfall—induced 2009 landslide at Marappalam area of Nilgiris district, Tamil Nadu state, India. Landslides. 2017;14:1803–14.
[6] Dang K, Sassa K, Konagai K, et al. Recent rainfall-induced rapid and long-traveling landslide on 17 May 2016 in Aranayaka, Kagelle District, Sri Lanka. Landslides. 2019;16:155–64.
[7] Raj M, Sengupta A. Rain-triggered slope failure of the railway embankment at Malda, India. Acta Geotechnica. 2014;9:789–98.
[8] Korup O, Seidemann J, Mohr CH. Increased landslide activity on forested hillslopes following two recent volcanic eruptions in Chile. Nat Geosci. 2019;12:284–9.
[9] Ibsen M-L, Casagli N. Rainfall patterns and related landslide incidence in the Porretta-Vergato region, Italy. Landslides. 2004;1:143–50.
[10] Wieczorek GF, Glade T. Climatic factors influencing occurrence of debris flows. In: Debris-flow hazards and related phenomena. Springer Praxis Books. Berlin, Heidelberg: Springer; 2005.
[11] Rahimi A, Rahardjo H, Leong EC. Effect of antecedent rainfall patterns on rainfall-induced slope failure. J Geotech Geoenviron Eng. 2011;137:483–91.
[12] Chen H, Wei L, Tan L. Review of research on empirical rainfall threshold of rainfall-induced Landslide. J Chongqing Jiaotong Univ. 2012.
[13] Segoni S, Piciullo L, Gariano SL. A review of the recent literature on rainfall thresholds for landslide occurrence. Landslides. 2018;15:1483–501.
[14] Tsaparas I, Rahardjo H, Toll DG, Leong EC. Controlling parameters for rainfall-induced landslides. Comput Geotech. 2002;29:1–27.
[15] Campbell RH. Soil slips, debris flows, and rainstorms in the Santa Monica Mountains and vicinity. Professional Paper. 1975.
[16] Lainas S, Sabatakakis N, Koukis G. Rainfall thresholds for possible landslide initiation in wildfire-affected areas of western Greece. Bull Eng Geol & Environ. 2016;75:1–14.
[17] Li C, Ma T, Zhu X, Li W. The power-law relationship between landslide occurrence and rainfall level. Geomorphology. 2011;130:221–9.
[18] Brunetti MT, Peruccacci S, Rossi M, Luciani S, Valigi D, Guzzetti F. Rainfall thresholds for the possible occurrence of landslides in Italy. Nat Hazards Earth Syst Sci. 2010;10:447–58.
[19] Vennari C, Gariano SL, Antronico L, et al. Rainfall thresholds for shallow landslide occurrence in Calabria, southern Italy. Nat Hazards Earth Syst Sci. 2014;14:317–30.
[20] Glade T, Crozier M, Smith P. Applying probability determination to refine landslide-triggering rainfall thresholds using an empirical "antecedent daily rainfall model". Pure Appl Geophys. 2000;157:1059–79.
[21] Dai FC, Lee CF. Frequency–volume relation and prediction of rainfall-induced landslides. Eng Geol. 2001;59:253–66.
[22] Huang J, Ju NP, Liao YJ, Liu DD. Determination of rainfall thresholds for shallow landslides by a probabilistic and empirical method. Nat Hazards Earth Syst Sci. 2015;15:2715–23.
[23] Brand EW, Premchitt J, Phillipson HB. Relationship between rainfall and landslides in Hong Kong. Proceedings of the 4th International Symposium on Landslides; 1984 01/01; USA. Toronto. p. 276–84.
[24] Reichenbach P, Cardinali M, Vita PD, Guzzetti F. Regional hydrological thresholds for landslides and floods in the Tiber River Basin (central Italy). Environ Geol. 1998;35:146–59.
[25] Jakob M, Weatherly H. A hydroclimatic threshold for landslide initiation on the North Shore Mountains of Vancouver, British Columbia. Geomorphology. 2003;54:137–56.
[26] Guzzetti F, Peruccacci S, Rossi M, Stark CP. Rainfall thresholds for the initiation of landslides in Central and Southern Europe. Meteorol & Atmos Phys. 2007;98:239–67.
[27] Dahal RK, Hasegawa S. Representative rainfall thresholds for landslides in the Nepal Himalaya. Geomorphology. 2008;100:429–43.
[28] Bai S, Jian W, Thiebes B, Cheng C, Yang Y. Analysis of the relationship of landslide occurrence with rainfall: A case study of Wudu County, China. Arab J Geosci. 2013;7:1277–85.
[29] Lazzari M, Piccarreta M, Capolongo D. Landslide Triggering and Local Rainfall Thresholds in Bradanic Foredeep, Basilicata Region (Southern Italy). In: Margottini C, Canuti P, Sassa K, eds. Landslide Science and Practice. Vol. 2, Early Warning, Instrumentation and Monitoring. Berlin, Heidelberg: Springer Berlin Heidelberg; 2013. p. 671–7.
[30] Althuwaynee OF, Pradhan B, Ahmad N. Estimation of rainfall threshold and its use in landslide hazard mapping of Kuala Lumpur metropolitan and surrounding areas. Landslides. 2015;12:861–75.
[31] Rosi A, Peternel T, Jemec-Auflič M, Komac M, Segoni S, Casagli N. Rainfall thresholds for rainfall-induced landslides in Slovenia. Landslides. 2016;13:1571–7.
[32] Chen C-W, Oguchi T, Hayakawa YS, Saito H, Chen H. Relationship between landslide size and rainfall conditions in Taiwan. Landslides. 2017;14:1235–40.
[33] Gao L, Zhang LM, Cheung RWM. Relationships between natural terrain landslide magnitudes and triggering rainfall based on a large landslide inventory in Hong Kong. Landslides. 2018;15:1–14.
[34] Althuwaynee O, Asikoglu O, Eris E. Threshold contour production of rainfall intensity that induces landslides in susceptible regions of Northern Turkey. Landslides. 2018;15:1541–60.

[35] Kanjanakul C, Chub-uppakarn T, Chalermyanont T. Rainfall thresholds for landslide early warning system in Nakhon Si Thammarat. Arab J Geosci. 2016;9:1–11.
[36] Chen Y, Irfan M, Uchimura T, Cheng G, Nie W. Elastic wave velocity monitoring as an emerging technique for rainfall-induced landslide prediction. Landslides. 2018;15:1155–72.
[37] Mirus BB, Becker RE, Baum RL, Smith JB. Integrating real-time subsurface hydrologic monitoring with empirical rainfall thresholds to improve landslide early warning. Landslides. 2018;15:1909–19.
[38] Sorbino G, Nicotera MV. Unsaturated soil mechanics in rainfall-induced flow landslides. Eng Geol. 2013;165:105–32.
[39] Napolitano E, Fusco F, Baum RL, Godt JW, Vita PD. Effect of antecedent-hydrological conditions on rainfall triggering of debris flows in ash-fall pyroclastic mantled slopes of Campania (southern Italy). Landslides. 2016;13:967–83.
[40] Suryo EA, Gallage C, Trigunarsyah B. A Method for Predicting Rain-induced Instability of an Individual Slope. International Conference of the International Institute for Infrastructure Renewal and Reconstruction; 2015.
[41] Chen LX, Yin KL, Liu LL, Zhou YC. Analysis of relationship between landslide and rainfall in Jiangxi Province. Rock & Soil Mech. 2008;29:1114–20.
[42] Ai-Hua Z. Study on geologic disaster status and formation mechanism in Wuyuan, Jiangxi Province (in Chinese). Resour Survey Environ. 2010;31:221–9.
[43] Yin KL. Prediction of landslide disaster. Wuhan, China: China University of Geosciences Press; 2004.
[44] Shan J. Rainfall characteristics analyses on landslide in Jiangxi Province. Meteorol Mon. 2004;30:13–6.
[45] Lai CH. Experimental study of stress-dependent soil-water characteristics and their applications on numerical analysis of slope stability. Slopes. 2004.
[46] Karube D, Kawai K. The role of pore water in the mechanical behavior of unsaturated soils. Geotech Geol Eng. 2001;19:211–41.
[47] Fredlund DG, Rahardjo H. Soil mechanics for unsaturated soils. Hoboken, New Jersey: Wiley & Sons Ltd; 1993.
[48] Kassim A, Gofar N, Lee LM, Rahardjo H. Modeling of suction distributions in an unsaturated heterogeneous residual soil slope. Eng Geol. 2012;131–132:70–82.
[49] Ran Q, Hong Y, Wei L, Gao J. A modelling study of rainfall-induced shallow landslide mechanisms under different rainfall characteristics. J Hydrol. 2018;563:790–801.
[50] Cascini L, Cuomo S, Pastor M, Sacco C. Modelling the post-failure stage of rainfall-induced landslides of the flow type. Can Geotech J. 2013;50:924–34.
[51] Ku C-Y, Liu C-Y, Su Y, Xiao J-E, Huang C-C. Transient modeling of regional rainfall-triggered shallow landslides. Environ Earth Sci. 2017;76(16):570.
[52] Lam L, Fredlund DG, Barbour SL. Transient seepage model for saturated–unsaturated soil systems: a geotechnical engineering approach. Rev Can Géotech. 2011;24:565–80.
[53] Fredlund DG, Xing A. Equations for the soil-water characteristic curve. Rev Can Géotech. 1994;31:521–32.